Journal of Hydroscience and Hydraulic Engineering
Vol. 18, No.1 May, 2000, 29-38

DEVELOPMENT OF AN ALGORITHM FOR SOIL MOISTURE MAPPING BASED ON SINGLE-PARAMETER SAR IMAGES IN PERMAFROST REGIONS INCLUDING THE EFFECT OF SURFACE ROUGHNESS

By

Takeo Tadono

National Space Development Agency of Japan, Roppongi, Minato-ku, Tokyo, Japan

Toshio Koike

Department of Civil Engineering, University of Tokyo, Bunkyo-ku, Tokyo, Japan

Jiancheng Shi

Institute for Computational Earth System Science, University of California, Santa Barbara, USA

Yongjian Ding, Xianzhang Chen, Shaoling Wang and Meixue Yang

Lanzhou Institute of Glaciology and Geocryology, Chinese Academy of Sciences, Lanzhou, China

SYNOPSIS

An algorithm was developed to map soil moisture using the spatial and temporal distributions of the microwave backscattering coefficients of the ground surface. A scattering model that includes the Integral Equation Method (IEM) was applied to the L-band Synthetic Aperture Radar (SAR) mounted on the Japanese Earth Resources Satellite-1 (JERS-1). The images used in this study were taken over the Tibetan Plateau in January and August 1993. The ground surface backscattering coefficient is affected not only by soil moisture but also by other factors, such as, surface roughness, vegetation, and soil composition. To obtain the values related to roughness, we conducted ground-based measurements in the summer of 1997 as a part of the Tibet regional experiment of the GEWEX Asian Monsoon Experiment (GAME) project. Two experiment areas with different surface characteristics were selected. We drew a surface roughness map from the January JERS-1 SAR image by applying the scattering model and the relationship between two surface roughness parameters obtained through the ground-based measurements. We also derived an August soil moisture map from the August image by applying the scattering model and the surface roughness map estimated in January. The estimated distributions of the soil moisture on the Tibetan Plateau qualitatively correspond to those obtained by field measurement.

INTRODUCTION

Soil moisture is a key parameter in numerous environmental studies, including hydrology, meteorology, and agriculture. It plays important roles in the interactions between the land surface and the atmosphere, as well as in the separation of precipitation into runoff and ground water storage. In spite of its importance, soil moisture is not generally used for weather forecasting and water resources management because it is difficult to measure on a routine basis over large areas. In cold regions, hydrological processes such as melting of snow and permafrost are considered to play predominant roles in global atmospheric circulation as well as the seasonal march and interannual variation of the regional climate. It has been suggested, for example, that the anomalous state of soil moisture on the Tibetan Plateau affects the variation of the Asian summer monsoon through the atmospheric heating processes over the plateau (Yasunari et al. (17)). Some algorithms were developed to estimate this important parameter on a large scale using brightness temperature data from passive microwave radiometer measurements (Jackson et al. (7), Njoku and Kong (10), Wang et al. (15)). Koike et al. (9) derived the spatial and seasonal distributions of surface soil wetness in the Eurasian Continent, especially in the east part of China and the Tibetan Plateau, from the Special Sensor Microwave Imager (SSM/I)

data. However, the main drawback of radiometer systems for understanding the effect of land surface hydrological heterogeneity on atmospheric circulation and management of basin-scale water resources is their coarse spatial resolution. Active microwave remote sensors, in particular Synthetic Aperture Radars (SARs), have the potential of observing surface soil moisture with high spatial resolution on a regional scale (Engman and Chauhan (3)).

The signal obtained by SAR is known as the backscattering coefficient and is affected by not only dielectric properties that depend on the soil moisture, but also on surface roughness, correlation length, and other surface characteristics. Previous studies (Dobson and Ulaby (2), Wang et al. (16)) have revealed that Shuttle Imaging Radar-B (SIR-B) imagery with single polarization and single frequency can only describe the dependence of backscattering coefficients on these surface parameters. Polarimetric radar data were acquired in the Shuttle Imaging Radar-C (SIR-C) experiment. More sophisticated algorithms for soil moisture were presented using these data (Oh et al. (11), Shi et al. (13)). However, no space-borne polarimetric SAR has become operational so far.

The objective of this study is to develop an algorithm for soil moisture mapping with fine spatial resolution by single-parameter SAR data. To compensate for the lack of information, we introduce regional characteristics of surface roughness and seasonal variation of soil moisture into a scattering model that includes the Integral Equation Method (IEM) (Fung et al. (4), Fung (5)). To reduce the number of unknown parameters, we parameterize the relationships between two roughness parameters through ground-based measurements.

DERIVATION

Basic Equations of Scattering Processes

The scattering model used in this study formulates scattering processes from an inhomogeneous medium composed of irregular soil particles and water. To apply this model to perfectly dry conditions, such as, permafrost regions in winter, we used the microwave radiative transfer model including both processes of surface and volume scattering for the half-space medium as formulated by

$$I\ (\mu_s,\phi_s) = I_s + I_{vt} \tag{1}$$

where $I\ (\mu_s,\phi_s)$ = total scattered intensity; $\mu_s = \cos(\theta_s)$; θ_s = scattering angle; ϕ_s = azimuth angle; I_{vt} = scattering intensity due primarily to volume scattering within the medium calculated based on the first-order radiative transfer solution; and I_s = surface scattering from the top boundary calculated by the IEM model (see Shi and Dozier (12)) that is,

$$\begin{aligned}\sigma^0_{pp} &= 4\pi\cos(\theta_s)\left[I_p(\mu_s,\phi_s)/I^i_p\right]\Big|_{\theta_s=\theta_i} \\ &= \frac{k^2}{2}\exp\left[-2k_z\sigma^2\right]\sum_{n=1}^{\infty}\left|I^n_{pp}\right|^2\frac{W^{(n)}(-2k_x,0)}{n!}\end{aligned} \tag{2}$$

with

$$I^n_{pp} = (2k_z\sigma)^n f_{pp}\exp\left[-2k_z^2\sigma^2\right] + \frac{1}{2}\left\{k_z^n\left[F_{pp}(-k_x,0)+F_{pp}(k_x,0)\right]\right\} \tag{3}$$

where subscript pp = polarization state ($p = h$ or v) and

$$f_{hh} = -2R_h/\cos(\theta_i) \tag{4}$$

$$f_{vv} = 2R_v/\cos(\theta_i) \tag{5}$$

$$F_{hh}(-k_x,0)+F_{hh}(k_x,0) = \frac{-2\sin^2(\theta_i)(1+R_h)^2}{\cos(\theta_i)}\left[\left(1-\frac{1}{\mu_r}\right)+\frac{\mu_r\varepsilon_s-\sin^2(\theta_i)-\mu_r\cos^2(\theta_i)}{\mu_r^2\cos^2(\theta_i)}\right] \tag{6}$$

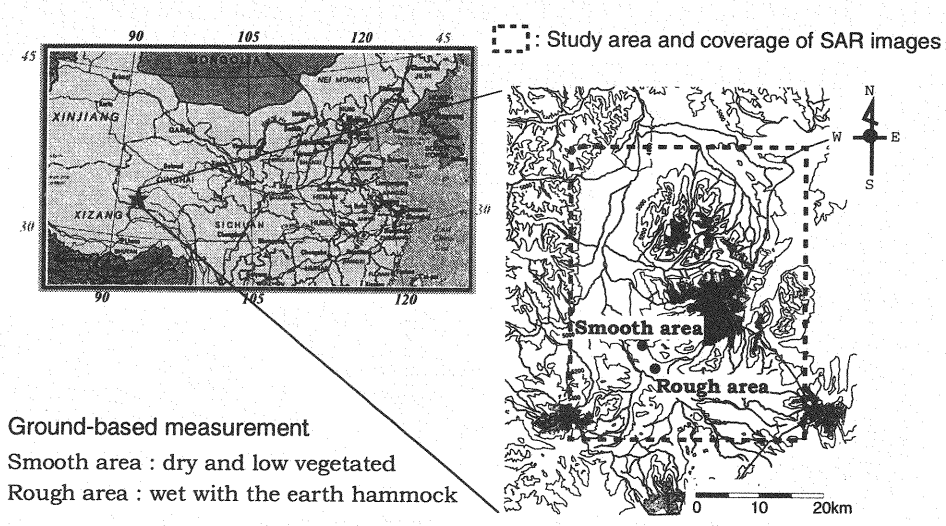

Fig. 1 Study area and location of two test sites

$$F_{vv}(-k_x,0)+F_{vv}(k_x,0)=\frac{2\sin^2(\theta_i)(1+R_v)^2}{\cos(\theta_i)}\left[\left(1-\frac{1}{\varepsilon_s}\right)+\frac{\mu_r\varepsilon_s-\sin^2(\theta_i)-\varepsilon_s\cos^2(\theta_i)}{\varepsilon_s^2\cos^2(\theta_i)}\right] \tag{7}$$

In the above equations, σ^0_{pp} = backscattering coefficient; I^i_p = transmitted intensity; θ_i = local incidence angle, if calculating backscattering for other than $\theta_i=\theta_s$; R_p = Fresnel reflection coefficient for p polarization; k = wave number depending on wavelength, λ; $k_z=k\cos(\theta_i)$; $k_x=k\sin(\theta_i)$; ε_s = relative complex dielectric constant of the surface; μ_r = relative magnetic permeability of the surface; σ = standard deviation of the surface height; and $W^{(n)}(-2k_x,0)$ = Fourier transform of the nth power of the surface correlation function, $\rho(\xi)$.

Algorithm Basis

Equation 1 input from Eq. 2 to Eq. 7 can be expressed simply as follows:

$$I\ (\mu_s,\phi_s)=f(\lambda, pp, P_t, \theta_s, \varepsilon_s, d, \sigma, l, n) \tag{8}$$

where P_t = transmitted power; d = diameter of soil particle; and l = correlation length of soil surface. Variables λ, pp and P_t are the system parameters, and θ_s is calculated using the Digital Elevation Model (DEM) and the satellite orbit information. We assume $n=1$, which corresponds to the exponential correlation function (see Fung (5)), to apply to L-band data with relatively longer wavelength than surface roughness scales. To evaluate ε_s, we use the semi-empirical model for a four-component mixture (see Dobson et al. (1)). That is,

$$\varepsilon_s=f(Mv, t, \rho_s, \alpha, \beta) \tag{9}$$

where Mv = volumetric water content of soil; t = thermometric temperature of soil medium; ρ_s = soil density; and α, β = ajustable parameters for soil composition. In this study, typical values of α and β for sandy soil are adapted. Parameters ρ_s and d are treated as fitting parameters. Temperature t is assumed to be -5 degree Celsius in winter and +10 degree Celsius in summer. Consenquently, Eq. 8 can be expressed as

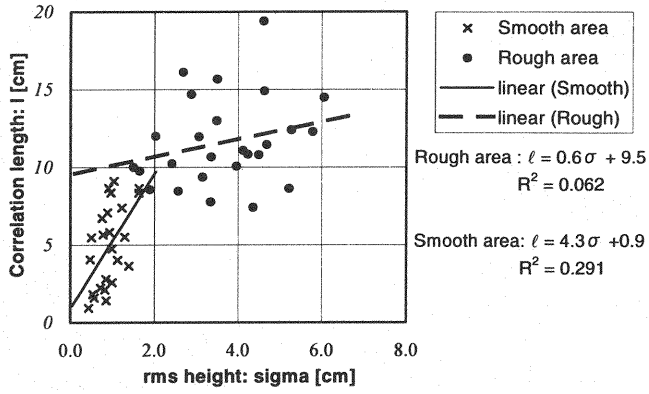

Fig. 2 Relationship between σ and l based on ground-based measurement

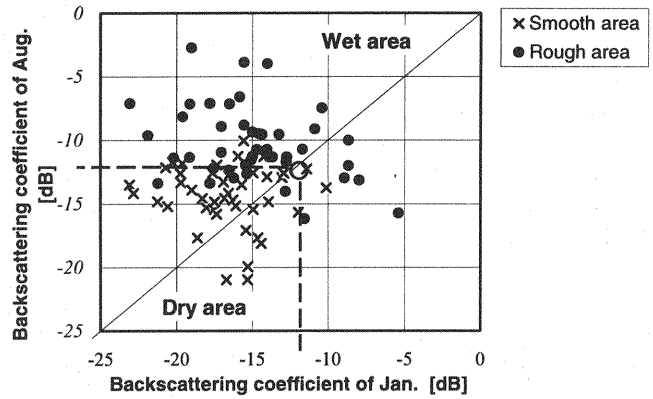

Fig. 3 Determination of the threshold value for classifying surface conditions

$$I\ (\mu_s, \phi_s) = f(Mv, \sigma, l) \tag{10}$$

There are three unknown parameters. To solve Eq. 10, we introduce relationships between two surface roughness parameters derived from field surveys and assume particular values for regional characteristics of soil moisture.

APPLICATION TO PERMAFROST REGION IN THE TIBETAN PLATEAU

Ground-based Measurements and Relationship between the Two Surface-Roughness Parameters

The surface roughness parameters were obtained as a part of the Tibet regional experiment of the GEWEX Asian Monsoon Experiment (GAME) project in the summer of 1997. Figure 1 shows the study area in the plateau. The two dots indicate test sites selected with different surface characteristics: one with short vegetation characterized as a relatively smooth surface, and the other, situated in an earth hammock area regarded as a relatively rough surface. They had typical surface conditions on the plateau.

We selected 12 measurement points in 60m square of each site. A total number of 24 one-dimensional profiles of the land surface height were measured by a comb-style instrument (from 40cm to 80cm length, 2mm interval) in each site (two profiles in different directions for each measured point). Two surface roughness parameters, standard deviation of height (σ) and surface correlation length (l), were calculated for each surface profile through Eq. 11 to Eq. 14 (see Ulaby et al. (14)).

$$\sigma = \left[\frac{1}{N-1} \left(\sum_{i=1}^{N} (Z_i)^2 - N(\bar{Z})^2 \right) \right]^{1/2} \tag{11}$$

$$\bar{Z} = \frac{1}{N} \sum_{i=1}^{N} Z_i \tag{12}$$

$$\rho(x') = \sum_{i=1}^{N+1-j} Z_i \, Z_{j+i-1} \Big/ \sum_{i=1}^{N} Z_i^2 \tag{13}$$

$$\rho(l) = 1/e \tag{14}$$

In these equations, Z_i = surface height at the location i; N = number of samples in a profile; $\rho(x')$ = normalized autocorrelation function; $x' = (j-1)\Delta x$; Δx = horizontal interval; and j = an integer $j \geq 1$. The results are shown in Fig. 2. To reduce the number of parameters contributing to backscattering coefficient, we assumed the following linear relationship between σ and l at each surface:

Smooth area $l = 4.3\sigma + 0.9$ (15)

Rough area $l = 0.6\sigma + 9.5$ (16)

The accuracy of the above assumptions was quite poor. However, these assumptions provided us the characteristics of surface roughness for each site. In addition, the sensitivity of the backscattering coefficient to the variation of σ exceeds the variation of l in the range of measured roughness based on numerical simulation using the single-scattering IEM model (see Shi et al. (13)). Therefore, we introduced the above roughness relationships into the algorithm and Eq. 10 was represented by

$$I\ (\mu_s, \phi_s) = f(Mv, \sigma(l)) \tag{17}$$

The land surfaces covered by SAR images were classified into the above two categories with certain threshold values decided statistically from the relationship of SAR-observed backscattering coefficients between January and August in the test sites (see Fig. 3). Equation 15 or 16 was applied to each pixel in the images depending on its category.

Calculation of Local Incidence Angle

Two L-band SAR images from the Japanese Earth Resources Satellite-1 (JERS-1), obtained in January and August under quite different hydrological conditions, were overlaid on a topographic map. This overlaid image is useful for qualitatively classifying the surface condition and detecting its seasonal change (see Koike et al. (8)). To determine the local incidence angle for each pixel, we calculated the normal unit vector of slope ($\vec{n}$) using four adjacent elevation data points derived from the DEM, Global Land One-kilometer Base Elevation (GLOBE) (see Fig. 4 and Ishidaira et al. (6)), which is a global-scale, high spatial resolution DEM. The area over 5,350 meters in elevation was masked out in this overlaid image as rocky surface. The incidence angle of JERS-1 SAR was defined at the center of the image. The coordinates of the image and topography map were matched. The local incidence angle ($\theta_i = \theta_s$) for all pixels was calculated by

$$\cos(\theta_s) = \vec{n} \cdot \vec{m} \tag{18}$$

where $\vec{m}$ = a unit vector along the backscattering direction (see Fig. 5). The geometric distortions, such as foreshortening and layover in the image, were not processed in this study because the area on the plateau was almost flat except for the mountainous region.

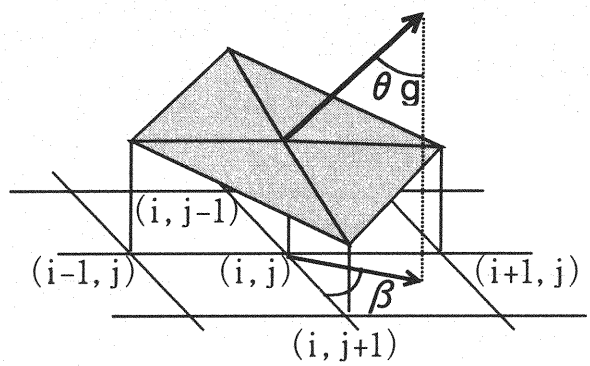

Fig. 4 Geometry of the normal unit vector of slope ($\vec{n}$)

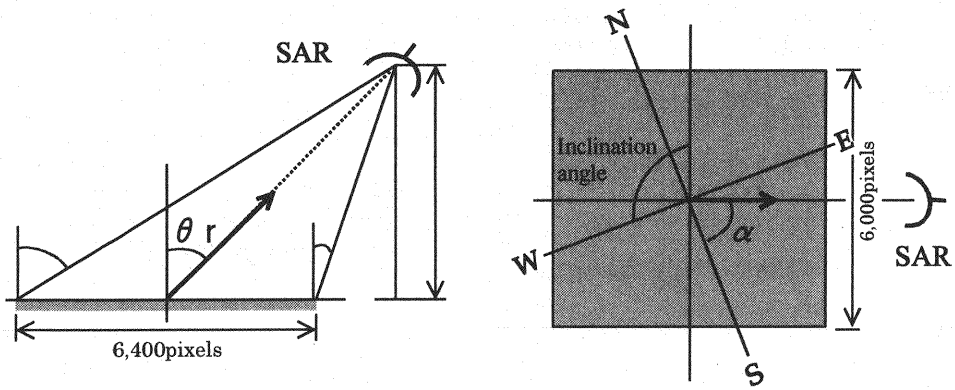

Fig. 5 Geometry of the unit vector of backscattering ($\vec{m}$)

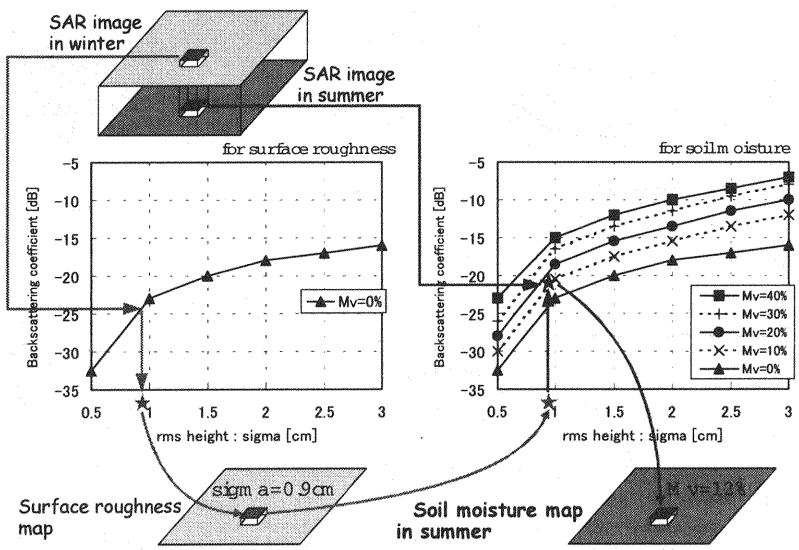

Fig. 6 Algorithm for estimating surface roughness and soil moisture for each pixel

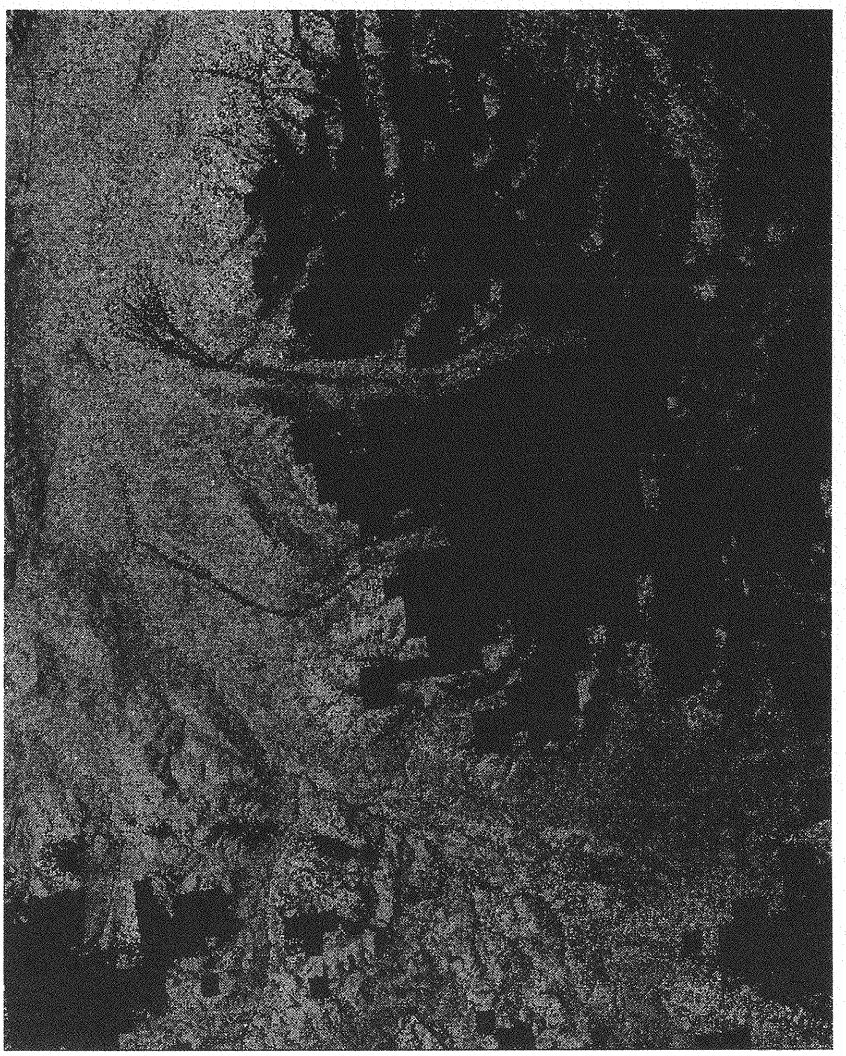

Fig. 7 50m mesh soil moisture map of the Tibetan Plateau by JERS-1 SAR image (Aug. 17, 1993)

Estimating Surface Roughness Distribution

Figure 6 shows the algorithm for estimating the surface roughness and soil moisture. By inputting the $\sigma - l$ relationships and the local incidence angles into the scattering model under dry conditions, we produced the distribution of surface roughness in January. The model was evaluated by both surface and volume scattering processes as in Eq. 1. In addition, there were usually snow-free in January except around mountaintops. The process was as follows:

1. Under assumed perfectly dry conditions due to subfreezing soil temperatures in winter, we simulate the backscattering coefficient as a function of incidence angle (θ_s) from 17 to 51 degrees with an interval of 2 degrees, the standard deviation of height (σ) from 0 to 2 cm with an interval of 1 mm for the smooth area, and from 0 to 7 cm with an interval of 2 mm for the rough area. We also made lookup tables for estimating $\sigma(l)$.
2. σ was derived from the simulated table by applying the combination of θ_s and the observed

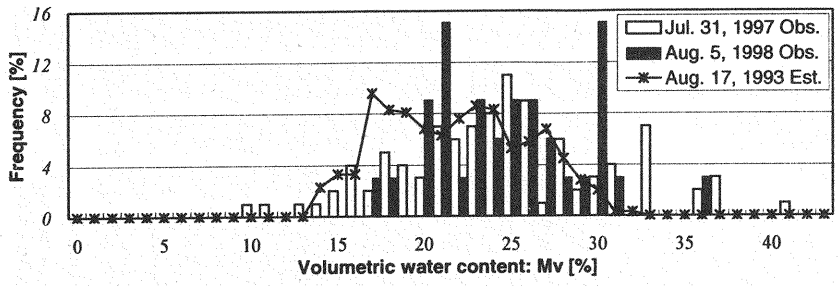

Fig. 8 Comparisons of soil water content histograms for smooth area estimated by this algorithm on August 17, 1993, and observed on July 31, 1997 and August 5, 1998

backscattering coefficient obtained on January 9, 1993.

3. The distribution of correlation length (l) was also derived.

Estimating Soil Moisture Distribution

In the Tibetan Plateau, soil moisture increases in summer because of rainfall and melting snow and permafrost. The soil moisture map in August was derived from the scattering model after inputting the local incidence angle and the distribution of roughness into it. The soil moisture distribution was estimated similarly to the roughness distribution.

1. The backscattering coefficient was simulated under various combinations of incidence angle (θ_s), standard deviation of height (σ), and soil moisture (Mv).
2. We estimated Mv for one pixel by using the observed backscattering coefficient obtained on August 17, 1993 and θ_s, and σ estimated from the January image.
3. Finally, we derived Mv map with a 50-meter mesh averaging over four pixels square of an original spatial resolution of 12.5 meters.

Results

Figure 7 shows the August soil moisture map obtained by this algorithm. The brighter portion of the image indicates the lower Mv ; darker, a higher Mv ; and black, the masking areas and areas out of the range of the lookup tables because the roughness is too large or small, such as a water surface. The surrounding areas of rivers and glacier tips have relatively high Mv values, and the lower right region in Fig. 7 is a very wet area. The estimated soil moisture distribution thus qualitatively corresponds to the result of the field examination. We could not directly compare absolute values of estimated soil moisture with measured ones because observation days were different. However, Fig. 8 compares histograms of soil moisture estimated this algorithm (solid line) and measured on July 31, 1997 (white boxes) and August 5, 1998 (black boxes) for a smooth area. Observed years were different, but the seasons were almost the same as the estimated one. The absolute values were different, but the shapes and range of distribution were similar to measured values.

CONCLUSION

This paper developed an algorithm for soil moisture mapping in the Tibetan Plateau by using two images of single-parameter L-band SAR. To reduce the number of unknown parameters contributing to the backscattering coefficient, we introduced regional characteristics of surface roughness and seasonal variation of soil moisture into a scattering model. The former was assumed through ground-based measurement under two typical types of surface conditions on the plateau. The latter was estimated using two temporal images obtained in winter and summer under quite different hydrological conditions. In winter, soil surface was perfectly dry because it was in a permafrost region. Thus, we considered evaluating not only surface scattering but also volume scattering in the model. In summer, soil moisture increases because of rainfall and melting snow and permafrost. The local incidence angle for each image pixel was also evaluated using DEM, GLOBE data.

We can conclude from this study that the algorithm derived can be applied to single-parameter SAR with the hydrological knowledge. We also showed the possibility of estimating spatial distributions of surface roughness and soil moisture. When a higher resolution DEM becomes available, the algorithm can be improved to calculate the local incidence angles and to perform geometric correction in images. Furthermore, the algorithm must be validated previously with ground-based measurements and estimated parameters from obtained L-band SAR data. Currently, no L-band SAR system is mounted on a satellite. In the near feature, satellite-based multi-parameter SAR data will be available. At least, this means that the single-parameter data can be used continuously. To best manage the limitations of satellite data, we will have to consider an algorithm applying both parameter data sets.

REFERENCES

1. Dobson, M.C., F.T. Ulaby, M. Hallikainen and M. El-Rayes : Microwave dielectric behavior of wet soil -Part II: Four-component dielectric mixing models, IEEE Trans. Geosci. Remote Sensing, Vol.GE-23, pp.35-46, 1985.
2. Dobson, M.C. and F.T. Ulaby : Active microwave soil moisture research, IEEE Trans. Geosci. Remote Sensing, Vol.GE-24, pp.23-36, 1986.
3. Engman, E.T. and N. Chauhan : Status of microwave soil moisture measurements with remote sensing, Remote Sens. Environ., Vol.51, pp.189-198, 1995.
4. Fung, A.K., Z. Li and K.S. Chen : Backscattering from a randomly rough dielectric surface, IEEE Trans. Geosci. Remote Sensing, Vol.33, pp.356-369, 1992.
5. Fung, A.K. : Microwave Scattering and Emission Models and Their Applications, Norwood, MA, Artech House, 1994.
6. Ishidaira, H., T. Koike, M. Lu and N. Hayakawa : Macro-scale modeling for shortwave radiation budget, in Proc. The 2nd Int'l Study Conf. on GEWEX in Asia and GAME, pp.315-318, 1995.
7. Jackson, T.J., T.J. Schmugge and J.R. Wang : Passive microwave sensing of soil moisture under vegetation canopies, Water Resour. Res., Vol.18, pp.1137-1142, 1982.
8. Koike, T., K. Seko, X. Chen, T. Tadono, K. Tamagawa, H. Igarashi and H. Takizawa : Monitoring ground surface condition on Tibetan Plateau by using satellite remote sensing, Bulletin of Glacier Research, Japanese Society of Snow and Ice, Vol.12, pp.95-104, 1994.
9. Koike, T., T. Tsukamoto, T. Kumakura and M. Lu : Spatial and seasonal distribution of surface wetness derived from satellite data, Proc. of the Int'l Workshop on Macro-Scale Hydrological Modeling, pp.87-90, 1996.
10. Njoku, E. and J. Kong : Theory of passive microwave remote sensing of near-surface soil moisture, J. Geophys. Res., Vol.82, pp.3108-3118, 1977.
11. Oh, Y., K. Sarabandi and F.T. Ulaby : An empirical model and inversion technique for radar scattering from bare soil surface, IEEE Trans. Geosci. Remote Sensing, Vol.30, pp.370-378, 1992.
12. Shi, J. and J. Dozier : Inferring snow wetness using C-Band data from SIR-C's polarimetric Synthetic Aperture Radar, IEEE Trans. Geosci. Remote Sensing, Vol.33, pp.905-914, 1995.
13. Shi, J. and J.R. Wang, A.Y. Hsu, P.E. O'Neill and E.T. Engman : Estimation of bare soil moisture and surface roughness parameter using L-band SAR image data, IEEE Trans. Geosci. Remote Sensing, Vol.35, pp.1254-1266, 1997.
14. Ulaby, F.T., R.K. Moore and A.K. Fung : Microwave Remote Sensing, Active and passive, Addison-Wesley, pp.816-921, 1982.
15. Wang, J.R., P.E. O'Neill, T.J. Jackson and E.T. Engman : Multifrequency measurements of the effects of soil moisture, soil texture, and surface roughness, IEEE Trans. Geosci. Remote Sensing, Vol.GE-21, pp.44-55, 1983.
16. Wang, J.R., E.T. Engman, J.C. Shiue, M. Rusek and C. Steinmeier : The SIR-B observations of microwave dependence on soil moisture, surface roughness and vegetation covers, IEEE Trans. Geosci. Remote Sensing, Vol.GE-24, pp.510-516, 1986.
17. Yasunari, T., A. Kitoh and T. Tokioka : Local and remote response to excessive snow mass over Eurasia appearing in the northern spring and summer climate, Journal of Meteorological Society of Japan, Vol.69, pp.473-487, 1991.

APPENDIX - NOTATION

The following symbols are used in this paper:

d = diameter of soil particle;
$I(\mu_s,\phi_s)$ = total scattered intensity;
I_p^i = transmitted intensity;
I_s = surface scattering intensity from the top boundary surface;
I_{vl} = volume scattering intensity within the medium;
j = integer $j \geq 1$ in Eq. 14;
k = wave number;
k_x = $k\sin(\theta_i)$;
k_z = $k\cos(\theta_i)$;
l = correlation length of soil surface;
Mv = volumetric water content of soil;
$\vec{m}$ = unit vector along the backscattering direction;
N = number of samples for surface height;
$\vec{n}$ = normal unit vector of slope;
P_t = transmitting power;
pp = polarization state ($p=h$ or v);
R_p = Fresnel reflection coefficient for p polarization;
t = thermometric temperature of soil medium;
$W^{(n)}(-2k_x,0)$ = Fourier transform of the nth power of the surface correlation function;
$x'=(j-1)\Delta x$ = distance in Eq. 14;
Z_i = surface height;
α, β = ajustable parameters for soil composition;
Δx = horizontal interval in Eq. 13;
ε_s = relative complex dielectric constant of the surface;
θ_i, θ_s = local incidence and scattering angles;
λ = wavelength;
μ_r = relative magnetic permiability of the surface;
μ_s = $\cos(\theta_s)$;
$\rho(x')$ = normalized autocorrelation function;
$\rho(\xi)$ = surface correlation function;
ρ_s = soil density;
σ = standard deviation of the surface height;
σ_{pp}^0 = backscattering coefficient; and
ϕ_s = azimuth angle.

(Received July 26, 1999 ; revised December 8, 1999)